IEEE Access
Multidisciplinary | Rapid Review | Open Access Journal

Date of publication xxxx 00, 0000, date of current version xxxx 00, 0000.

Digital Object Identifier 10.1109/ACCESS.2017.DOI

Super Twisting-Based Nonlinear Gain Sliding Mode Controller for Position Control of Permanent-Magnet Synchronous Motors

JEONGHWAN GIL[1], SESUN YOU [1],YOUNGWOO LEE [2] AND WONHEE KIM.[3],

[1]Department of Energy Systems Engineering, Chung-Ang University, Seoul, 06974, Korea (e-mail: jhgil@cau.ac.kr, yousesun@cau.ac.kr)
[2]Department of Electrical Engineering, Chonnam National University, Gwangju 61186, Korea (e-mail: stork@jnu.ac.kr)
[3]School of Energy Systems Engineering, Chung-Ang University, Seoul, 06974, Korea (e-mail: whkim79@cau.ac.kr)

Corresponding author: Wonhee Kim (e-mail: whkim79@cau.ac.kr).

ABSTRACT This paper proposes a super twisting-based nonlinear gain sliding mode controller (STNGSMC) to achieve the position control of permanent-magnet synchronous motors (PMSMs). Nonlinear gain is developed to improve the position tracking performance of a super twisting sliding mode controller (STSMC). The inclusion of nonlinear gain in the STSMC reduces chattering, and the stability of the closed loop is mathematically proven using the Lyapunov theorem considering load torque. In the proposed method, chattering is analyzed using the describing function method under unmodeled dynamics, such as that corresponding to the quantization effect of the digital sensor, sensor resolution, and pulse-width modulation (PWM) switching noise, in PMSM position control systems. Consequently, the STNGSMC can improve the position tracking performance in steady-state responses. The performance of the proposed method is verified using simulations. The experimental results demonstrate that chattering can be reduced by the STNGSMC, consequently improving the position tracking performance.

INDEX TERMS Super twisting algorithm, sliding mode controller, position control, permanent-magnet synchronous motors.

I. INTRODUCTION

PERMANENT-magnet synchronous motors (PMSMs) are widely used in industrial applications owing to their high power density, high efficiency, and enhanced reliability. In addition, classical control methods such as proportional-integral (PI) control and proportional-integral-derivative control are used for PMSMs owing to their ease of implementation [1], [2]. However, these classical control methods cannot achieve good tracking performance owing to system nonlinearities and parameter variations over a wide operating range or external disturbances.

Various nonlinear control methods have been studied to improve the control performance of PMSMs. A nonlinear control method for field-weakening control and field-oriented control was proposed in [3]. An adaptive control algorithm was developed to enable speed tracking and minimize torque ripple [4]. In addition, an internal model principle-based controller was proposed to reduce sideband harmonics in PMSMs with low-switching-frequency inverters [5]. In [6], an adaptive law with type-2 fuzzy logic systems was designed to compensate for interconnection effects, reconstruction errors, and unknown functions. In [7], an adaptive fuzzy controller was designed to compensate for the dynamic uncertainty and external load effect in the speed loop of PMSM drives. A backstepping control law with an extended state observer was designed with input-output linearization in [8]. A nonlinear disturbance observer-based robust backstepping compensator was designed for a position controller under a lumped unknown disturbance in [9]. In [10], a predictive algorithm using integration was designed with respect to time step and ramp reference signals considering constraints such as field weakening and current limitations. Model predictive direct speed control was studied to overcome the limitations of cascaded linear controllers and online predictions in [11]. A position tracking controller was designed to minimize the quadratic index, and a recurrent wavelet-based Elman neural

This article has been accepted for publication in a future issue of this journal, but has not been fully edited. Content may change prior to final publication. Citation information: DOI 10.1109/ACCESS.2021.3121127, IEEE Access

network was developed to improve control performance and achieve robustness in [12]. These control methods have been improved to achieve tracking performance in PMSMs from different perspectives.

Sliding mode control (SMC) methods have been widely implemented in PMSM control systems because of their robustness and fast response [13]–[17]. However, chattering is a major disadvantage associated with SMC, and various methods have been studied to eliminate or reduce chattering. The signum function is replaced by certain smooth approximations such as tangent, saturation, and hyperbolic functions. A singular-perturbation-theory-based SMC was applied to the position tracking control of PMSMs in [18]. A boundary layer integral SMC was designed based on a quasi-linearized and decoupled model in [19]. These studies used approximation functions in the control scheme to reduce chattering. However, asymptotic stability cannot be ensured using approximation functions. Thus, the convergence of the steady-state error to zero cannot be mathematically verified. Adaptive SMC and iterative learning control were designed to ensure fast response and robustness and to reduce periodic torque ripples in [20]. However, the adaptive SMC method is required because of the the long learning time required to achieve robustness and fast response. To improve both chattering and finite reaching time, high-order sliding mode control (HOSMC) was developed in [21]. In particular, super twisting algorithm-based HOSMC has been commonly used to reduce chattering and achieve a finite reaching time [22], [23]. Several super twisting sliding mode controllers (STSMCs) have been developed to improve the control of the PMSM [24]–[26]. The STMSC mathematically verifies the reduction in chattering, but chattering still appears owing to the unmodeled dynamics, the quantization effect of the digital sensor, sensor resolution, and PWM switching noise. Thus, several STSMC methods have been developed to reduce chattering using the upper-bound function of the disturbance [27], [28]. However, determining the upper-bound function of the disturbance is difficult.

This paper proposed a super twisting-based nonlinear gain sliding mode controller (STNGSMC) to achieve position control of PMSMs. A nonlinear gain is developed to improve the position tracking performance of the STSMC. The inclusion of nonlinear gain in the STSMC reduces chattering, which is analyzed using the describing function method under various unmodeled dynamics in PMSM position control systems. Consequently, the STNGSMC can improve the position tracking performance in the steady-state responses. We mathematically prove the stability of closed-loop systems using the Lyapunov theorem and verify the performance of the proposed method via simulations and experiments.

II. SUPER TWISTING NONLINEAR GAIN SLIDING MODE CONTROLLER IN PMSM

Using a direct-quadrature transformation, the mathematical model of the PMSM can be represented in the state-space form [1] as follows:

$$\begin{aligned}\dot{\theta} &= \omega \\ \dot{\omega} &= -\frac{B}{J}\omega + \frac{K_m}{J} i_q - \frac{\tau_L}{J} \\ \dot{i}_d &= \frac{1}{L}(-R i_d + P\omega L i_q + v_d) \\ \dot{i}_q &= \frac{1}{L}(-R i_q - K_E\omega - P\omega L i_d + v_q)\end{aligned} \tag{1}$$

where v_d and v_q are the direct and quadrature voltages [V], respectively; i_d and i_q are the direct and quadrature currents [A], respectively; θ is the rotor (angular) position [rad]; ω is the rotor (angular) velocity [rad/s]; B is the viscous friction [N·m·s/rad]; J is the inertia of the motor [kg·m^2/rad]; R is the phase resistance [Ω]; L is the phase inductance [H]; P is the pole pair; K_m is the torque constant [rad/s/A]; K_E is the back-EMF constant [V·s/rad]; and τ_L is the load torque [N·m] and is assumed to be constant.

Mechanical tracking errors are defined as follows:

$$\begin{aligned}e_\theta &= \theta_d - \theta \\ e_\omega &= \omega_d - \omega\end{aligned} \tag{2}$$

where θ_d is the desired position, and $\omega_d = \dot{\theta}_d$ is the desired velocity. From (1) and (2), the tracking error dynamics are obtained as follows:

$$\begin{aligned}\dot{e}_\theta &= e_\omega \\ \dot{e}_\omega &= \dot{\omega}_d + \frac{B}{J}\omega - \frac{K_m}{J} i_q + \frac{\tau_L}{J}.\end{aligned} \tag{3}$$

A sliding surface, s, is defined as follows:

$$s = k_1 e_\theta + k_2 e_\omega \tag{4}$$

where k_1 and k_2 are positive constants, and the derivative of the sliding surface is derived as follows:

$$\begin{aligned}\dot{s} &= k_1 \dot{e}_\theta + k_2 \dot{e}_\omega \\ &= k_1 e_\omega + k_2 \left(\dot{\omega}_d + \frac{B}{J}\omega - \frac{K_m}{J} i_q + \frac{\tau_L}{J} \right).\end{aligned} \tag{5}$$

A. WITHOUT LOAD TORQUE

If the load torque is assumed to be zero, the control input of the proposed controller for the mechanical dynamics is designed as follows:

$$i_q = u_{eq} + \frac{J}{K_m} \left(\frac{\lambda_1}{k_2} \sqrt{s^2 + \gamma |s|}\, \mathrm{sgn}(s) - u_i \right) \tag{6}$$

where

$$\begin{aligned}u_{eq} &= \frac{J}{K_m} \left(\frac{k_1}{k_2} e_\omega + \dot{\omega}_d + \frac{B}{J}\omega \right) \\ \dot{u}_i &= -\lambda_2\, \mathrm{sgn}(s).\end{aligned} \tag{7}$$

λ_1 and λ_2 are positive constant numbers, and $0 < \gamma < 1$.

Substituting the control inputs, (6) and (7), into (5), the derivative of the sliding surface becomes

$$\begin{aligned}\dot{s} &= -\lambda_1 \sqrt{s^2 + \gamma |s|}\, \mathrm{sgn}(s) + u_i \\ \dot{u}_i &= -\lambda_2\, \mathrm{sgn}(s).\end{aligned} \tag{8}$$

This article has been accepted for publication in a future issue of this journal, but has not been fully edited. Content may change prior to final publication. Citation information: DOI 10.1109/ACCESS.2021.3121127, IEEE Access

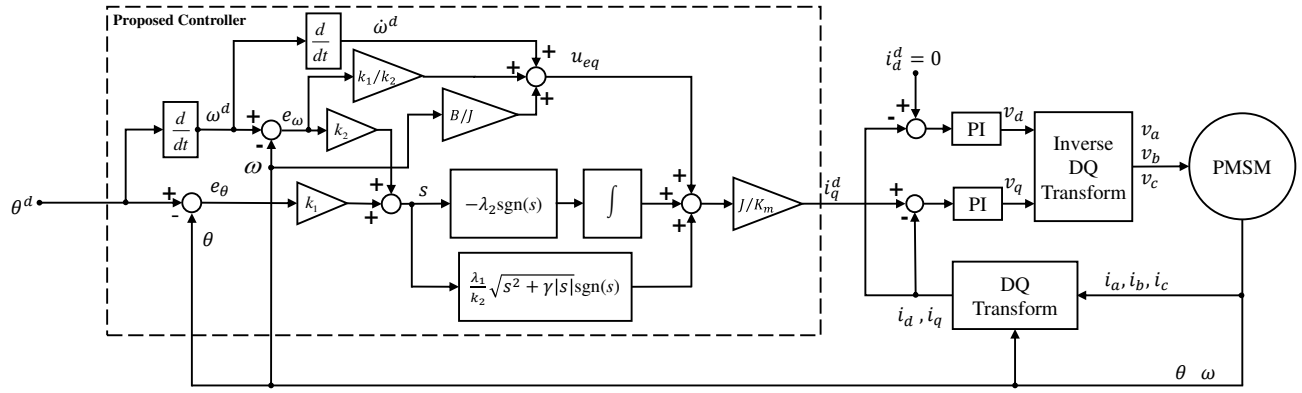

FIGURE 1: Block diagram of the overall system model

The stability of the proposed method was proven using the Lyapunov theory. The auxiliary state variables are defined as follows:

$$\begin{aligned}\zeta_1 &= \sqrt{s^2+\gamma|s|}\,\mathrm{sgn}(s)\\ \zeta_2 &= u_i.\end{aligned} \tag{9}$$

The dynamics of auxiliary state variables are defined as follows:

$$\begin{aligned}\dot{\zeta}_1 &= \frac{2|s|+\gamma}{2\sqrt{s^2+\gamma|s|}}(-\lambda_1\sqrt{s^2+\gamma|s|}\,\mathrm{sgn}(s)+\zeta_2)\\ \dot{\zeta}_2 &= -\lambda_2\,\mathrm{sgn}(s).\end{aligned} \tag{10}$$

The dynamics of auxiliary state variables are rewritten as follows:

$$\dot{\zeta} = \frac{1}{|\zeta_1|}A\zeta + \frac{|s|}{|\zeta_1|}R\zeta \tag{11}$$

where

$$A = \begin{bmatrix}\frac{-\gamma\lambda_1}{2} & \frac{1}{2}\\ -\lambda_2 & 0\end{bmatrix}, \quad R = \begin{bmatrix}-\lambda_1 & 1\\ 0 & 0\end{bmatrix}. \tag{12}$$

λ_1 and λ_2 are selected such that A is Hurwitz. The Lypunov candidate function, V, is defined as follows:

$$V = \zeta^T P\zeta \tag{13}$$

where P is a positive definite such that $A^TP+PA=-I$. The derivative of (13) is derived as follows:

$$\begin{aligned}\dot{V} &= \frac{1}{|\zeta_1|}\zeta^TA^TP\zeta + \frac{1}{|\zeta_1|}\zeta^TPA\zeta\\ &+ \frac{|s|}{|\zeta_1|}\zeta^TR^TP\zeta + \frac{|s|}{|\zeta_1|}\zeta^TPR\zeta\\ &= \frac{1}{|\zeta_1|}\zeta^T(A^TP+PA)\zeta + \frac{|s|}{|\zeta_1|}\zeta^T(R^TP+PR)\zeta.\end{aligned} \tag{14}$$

In (13), P is designed as follows:

$$P = \begin{bmatrix}p_{11} & p_{12}\\ p_{12} & p_{22}\end{bmatrix} \succ 0. \tag{15}$$

where

$$p_{11} = \frac{1+2\lambda_2}{\lambda_1\gamma}, \quad p_{12} = -1, \quad p_{22} = \frac{\lambda_1\gamma}{2\lambda_2} + \frac{1+2\lambda_2}{2\lambda_1\gamma\lambda_2}. \tag{16}$$

With (15) and (16), $\dot{V}$ becomes

$$\dot{V} = -\frac{1}{|\zeta_1|}\|\zeta\|^2 + \frac{|s|}{|\zeta_1|}\zeta^T(R^TP+PR)\zeta \tag{17}$$

where

$$R^TP+PR = \begin{bmatrix}r_1 & r_2\\ r_2 & r_3\end{bmatrix} \tag{18}$$

$r_1 = -\frac{2(1+2\lambda_2)}{\gamma}$, $r_2 = \lambda_1 + \frac{1+2\lambda_2}{\gamma\lambda_1}$, and $r_3 = -2$. The symmetric matrix R^TP+PR is semi-negative definite if and only if

$$\begin{aligned}r_1 &\le 0\\ r_1r_3 - r_2^2 &\le 0.\end{aligned} \tag{19}$$

Condition (19) can be rewritten as

$$\begin{aligned}-\frac{2(1+2\lambda_2)}{\gamma} &\le 0\\ -\left(\lambda_1 - \frac{1+2\lambda_2}{\gamma\lambda_1}\right)^2 &\le 0.\end{aligned} \tag{20}$$

The first condition can be satisfied with $(1+2\lambda_2)\ge 0$ because $0<\gamma<1$. The second condition is always satisfied for both λ_1 and λ_2. Consequently, if λ_1 and λ_2 are selected such that A is Hurwitz, and $(1+2\lambda_2)\ge 0$, we have

$$\dot{V} \le -\frac{1}{|\zeta_1|}\|\zeta\|^2. \tag{21}$$

Thus, ζ converges to zero in a finite time.

This article has been accepted for publication in a future issue of this journal, but has not been fully edited. Content may change prior to final publication. Citation information: DOI 10.1109/ACCESS.2021.3121127, IEEE Access

B. WITH LOAD TORQUE

In this section, the stability is proven for the load torque. With the load torque, the dynamics of the sliding surface are derived as follows:

$$\begin{aligned}\dot{s} &= k_1\dot{e}_\theta + k_2\dot{e}_\omega \\ &= k_1 e_\omega + k_2\left(\dot{\omega}_d + \frac{B}{J}\omega - \frac{K_m}{J}i_q + d\right).\end{aligned} \tag{22}$$

where d is the load term, $d = -\frac{\tau_L}{J}$. Thus, (22) with (6) can be rewritten as follows:

$$\begin{aligned}\dot{s} &= -\lambda_1\sqrt{s^2+\gamma|s|}\,\mathrm{sgn}(s) + u_i + d \\ \dot{u}_i &= -\lambda_2\,\mathrm{sgn}(s).\end{aligned} \tag{23}$$

Let us define $z := u_i + d$; then, $\dot{z} := \dot{u}_i + \dot{d}$ and the system can be written as

$$\begin{aligned}\dot{s} &= -\lambda_1\sqrt{s^2+\gamma|s|}\,\mathrm{sgn}(s) + z \\ \dot{z} &= -\lambda_2\,\mathrm{sgn}(s) + \dot{d}.\end{aligned} \tag{24}$$

Because $\dot{d} = 0$, (24) becomes

$$\begin{aligned}\dot{s} &= -\lambda_1\sqrt{s^2+\gamma|s|}\,\mathrm{sgn}(s) + z \\ \dot{z} &= -\lambda_2\,\mathrm{sgn}(s).\end{aligned} \tag{25}$$

Because (25) is equivalent to (8), it can be proven that the sliding surface, s, also converges to zero in finite time by the same procedure.

After the sliding surface, s, reaches zero, then

$$0 = k_1 e_\theta + k_2 e_\omega. \tag{26}$$

Consequently, the position tracking error exponentially converges to zero as follows:

$$\dot{e}_\theta = -\frac{k_1}{k_2}e_\theta. \tag{27}$$

A block diagram of the overall system and controller is shown in Fig. 1. The proposed methods (4), (6), and (7), which are shown in Fig. 1, generates the current input i_q. The PI controllers are implemented for current-loop in the PMSMs. The control gain tuning guide is as follows:

- λ_1 and λ_2 are selected such that A is Hurwitz and $(1+2\lambda_2) \geq 0$ for the stability.
- The positive constant γ was selected to be less than 1 to reduce chattering.

III. ANALYSIS OF CHATTERING PHENOMENON

This section examines chattering in STSMC, STNGSMC, and SMC under unmodeled dynamics in PMSM control systems. In [29], the chattering analysis is proven by describing the function method with unmodeled dynamics. The block diagram for the sliding surface dynamics, (8), in the presence of the unmodeled dynamics is shown in Fig. 2. In Fig. 2, p is the Laplace operator, μ is the unmodeled dynamics, and the function of Ω is defined as follows:

$$\Omega = \lambda_1\sqrt{s^2+\gamma|s|}\,\mathrm{sgn}(s). \tag{28}$$

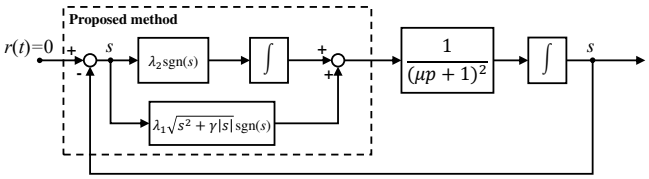

FIGURE 2: Block diagram of proposed method with unmodeled dynamics

Following the describing function method, the chattering of the sliding surface is considered to be $A\sin(\omega t)$, and the input of the nonlinearity is approximated as

$$u = \frac{a_0}{2} + a_1\cos(\omega t) + b_1\sin(\omega t). \tag{29}$$

The switching function, $\mathrm{sgn}(*)$, is an odd function, and the parameters of (29) are defined as follows:

$$a_0 = a_1 = 0. \tag{30}$$

Therefore, (29) is rewritten as follows:

$$u = b_1\sin(\omega t) \tag{31}$$

where b_1 is given by the input of the controllers shown in Fig. 2 such as $\lambda_2\,\mathrm{sgn}(s)$ and $\lambda_1\sqrt{s^2+\gamma|s|}\,\mathrm{sgn}(s)$. The sliding surface is considered as, $A\sin(\omega t)$, where b_1 is given by

$$\begin{aligned}b_1 &= b_{11} + b_{12} \\ b_{11} &= \frac{1}{\pi}\int_{-\pi}^{\pi}\lambda_2\,\mathrm{sgn}(A\sin(\delta))\sin(\delta)\,d\delta \\ b_{12} &= \frac{2}{\pi}\int_{0}^{\pi}\lambda_1\sqrt{A^2\sin^2(\delta)+\gamma|A\sin(\delta)|}\,\mathrm{sgn}\,\delta\sin(\delta)\,d\delta.\end{aligned} \tag{32}$$

Using inequalities such as $a^2+b^2 \geq 2ab$ and $\mathrm{sgn}(A\sin(\delta))\sin(\delta) = \sin(\delta)$, the equation for b_1 is rewritten as follows:

$$\begin{aligned}b_{11} &= \frac{4\lambda_2}{\pi} \\ b_{12} &> \frac{\lambda_1}{\pi}\int_0^{\pi} 2A\sin^2(\delta)+\gamma\sin(\delta)\,d\delta = \lambda_1 A + \frac{2\lambda_1\gamma}{\pi}.\end{aligned} \tag{33}$$

To obtain the describing function, b_1 is divided by A, that is given by

$$\begin{aligned}N_{11}(A) &= \frac{4\lambda_2}{\pi A} \\ N_{12}(A) &> \lambda_1 + \frac{2\lambda_1\gamma}{\pi A}.\end{aligned} \tag{34}$$

The transfer function of the sliding surface with unmodeled dynamics is given by

$$G(p) = \frac{1}{p(\mu p+1)^2}. \tag{35}$$

Replacing the Laplace parameter p by $j\omega$ yields

$$G(j\omega) = \frac{1}{j\omega(\mu j\omega+1)^2}. \tag{36}$$

This article has been accepted for publication in a future issue of this journal, but has not been fully edited. Content may change prior to final publication. Citation information: DOI 10.1109/ACCESS.2021.3121127, IEEE Access

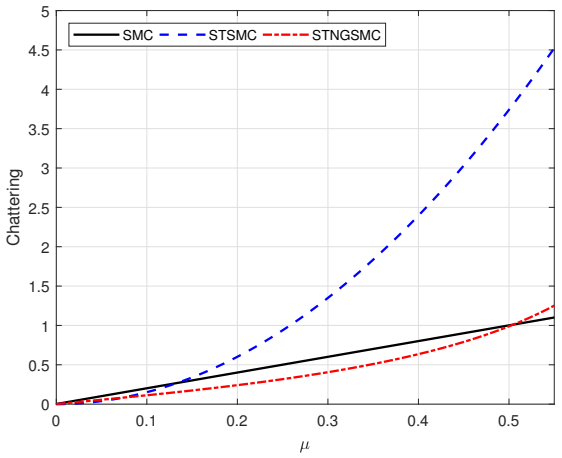

FIGURE 3: Chattering amplitude by unmodeled dynamics

The inverse transfer function of the sliding surface with unmodeled dynamics, $g(j\omega) = \frac{1}{G(j\omega)}$, is given as follows:

$$g(j\omega) = -(2\mu\omega^2) - j(\mu^2\omega^3 - \omega). \tag{37}$$

To complete the analysis, equating $N(A)$ to $-g(j\omega)$ is derived as

$$\frac{4\lambda_2}{\pi A p} + \lambda_1 + \frac{2\lambda_1\gamma}{\pi A} = (2\mu\omega^2) + j(\mu^2\omega^3 - \omega). \tag{38}$$

If the imaginary part of (38) is equal to zero, ω is calculated as follows:

$$\omega = -\frac{1}{3\mu}\left(\frac{27\mu^4 4\lambda_2 + \sqrt{(27\mu^4 4\lambda_2)^2 - 4(3\mu^2)^3}}{2}\right)^{\frac{1}{3}} - \frac{1}{3\mu}\left(\frac{27\mu^4 4\lambda_2 - \sqrt{(27\mu^4 4\lambda_2)^2 - 4(3\mu^2)^3}}{2}\right)^{\frac{1}{3}}. \tag{39}$$

Therefore, A, which is chattering amplitude, is rewritten as

$$A = \frac{2\lambda_1\gamma\omega}{-\lambda_1\pi\omega + 2\mu\pi\omega^3}. \tag{40}$$

Substituting (39) into (40), the chattering amplitude of the sliding surface under unmodeled dynamics is obtained. According to [29], the chattering of SMC and STSMC are calculated as

$$A_1 = \frac{2\mu\lambda_2}{\pi}$$
$$A_2 = \frac{\mu^2(\pi\lambda_1^2 + 16\lambda_2)^2}{4\lambda_1^2\lambda_2^2} \tag{41}$$

where A_1 is the chattering of SMC, and A_2 is the chattering of STSMC.

The chattering of SMC, STSMC, and STNGSMC is represented graphically in Fig. 3. The chattering amplitude of the STSMC is greater than that of the conventional SMC when $\mu > 0.15$. However, the chattering amplitude of the STNGSMC is less than that of the conventional SMC under the condition of $\mu < 0.5$.

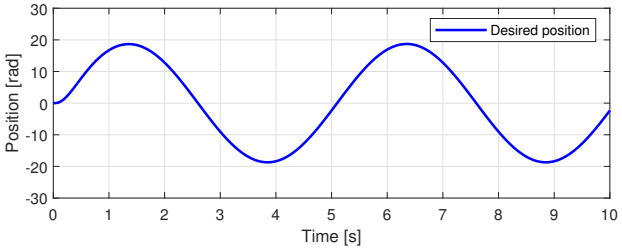

FIGURE 4: Position reference

IV. SIMULATION AND EXPERIMENTAL RESULTS

Simulations and experiments were conducted to validate the performance of the proposed STNGSMC. For comparison, the STSMC input was used for Case 1 as follows:

$$\begin{aligned} i_{q,1} &= u_{eq} + \frac{J}{K_m}\left(\frac{\lambda_1}{k_2}\sqrt{|s|}\,\mathrm{sgn}(s) + u_i\right) \\ u_{eq} &= \frac{J}{K_m}\left(\frac{k_1}{k_2}e_\omega + \dot{\omega}_d + \frac{B}{J}\omega\right) \\ \dot{u}_i &= \lambda_2\,\mathrm{sgn}(s). \end{aligned} \tag{42}$$

The STNGSMC input, (6) and (7), were implemented for Case 2. The smooth start sinusoidal signal $\theta^d = 6\pi(1 - e^{-5t})\sin(0.4\pi t)$ rad was used as the desired position in the simulations and experiments, as shown in Fig. 4. The desired position is used for the industrial servo system to prevent the peaking phenomenon. The nominal parameters listed in Table 1 were used for the PMSM in the simulations and experiments. The control gains listed in Table 1 were implemented for Cases 1 and 2. An initial position displacement, i.e., $\theta(0) = -0.008$ rad, was set to study the transient response.

TABLE 1: Nominal PMSM parameters and control gains

Parameter	Value	Gain	Value
J	4.675×10^{-4}[kg·m^2/rad]	k_1	200
B	3.7×10^{-3}[N·m·s/rad]	k_2	0.5
R	0.2 [Ω]	λ_1	2100
L	0.4×10^{-3}[H]	λ_2	1000
K_m	0.102 [V·s/rad]	γ	0.5

A. SIMULATION RESULTS

Simulations were conducted using MATLAB/Simulink to validate the performance of the proposed method. The control gains and parameters are listed in Table 1. In the simulation, the parameter uncertainties, which are a maximum of ±20 % from the nominal value of Table 1, were applied to verify the robustness of STSMC and STNGSMC. The sliding surfaces of Cases 1 and 2 are shown in Fig. 5. The initial position displacement generated a transient response, where it was observed that the finite reaching time of STSMC is as shown in Fig. 5 (b). After observing the finite reaching time, chattering was observed for STSMC and STNGSMC, as shown in Fig. 5 (c). The chattering in Case 2 was reduced

This article has been accepted for publication in a future issue of this journal, but has not been fully edited. Content may change prior to final publication. Citation information: DOI 10.1109/ACCESS.2021.3121127, IEEE Access

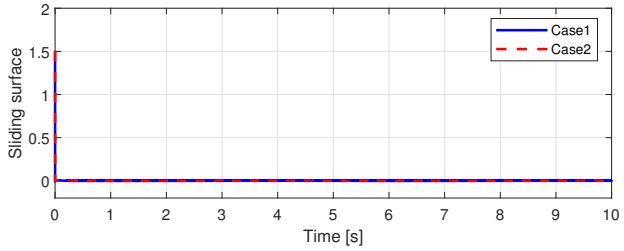

(a) Sliding surfaces s

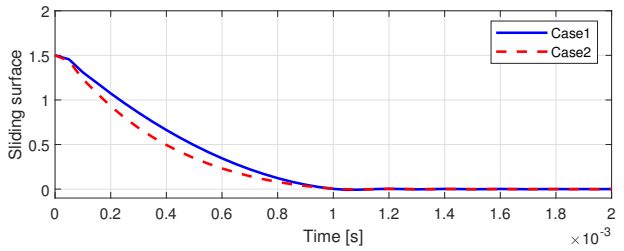

(b) Enlarged sliding surface in the transient response

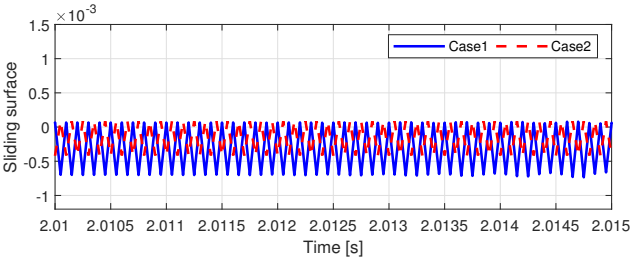

(c) Enlarged sliding surface in the steady-state response

FIGURE 5: Sliding surfaces in simulations

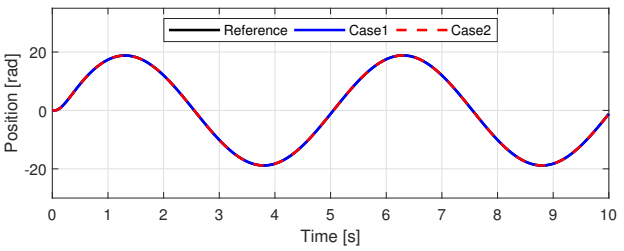

(a) Position tracking performances

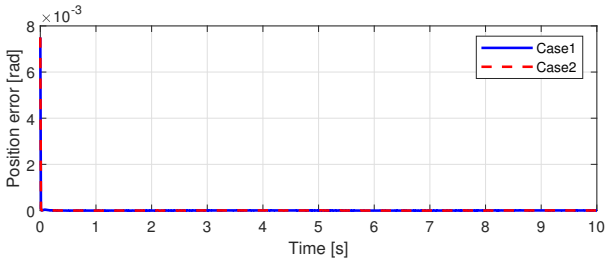

(b) Position tracking errors

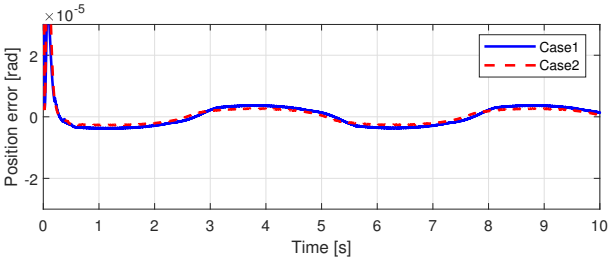

(c) Enlarged position tracking errors

FIGURE 6: Position tracking performances in simulations

by STNGSMC. The position tracking performances of Cases 1 and 2 are shown in Fig. 6. The chattering of the sliding surface near the origin affected the position tracking performances of Cases 1 and 2. Therefore, we can observe that the ripple of the position of Case 2 was smaller than that of Case 1, as shown in Fig. 6 (c). The current inputs for Cases 1 and 2 are shown in Fig. 7. There were fewer fluctuations in the current input in Case 2 owing to the reduced chattering.

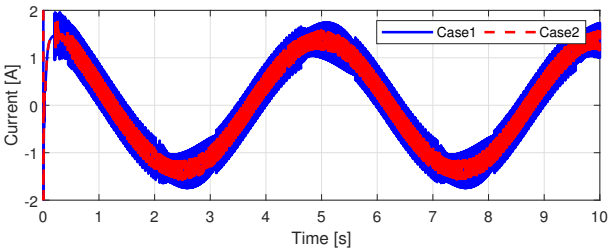

FIGURE 7: Current inputs in simulations

B. EXPERIMENTAL RESULTS

Experiments were performed using a PMSM testbed, which consisted of ControlDesk, two RapidPro units, and a SCALEXIO real-time system, as shown in Fig. 8, to validate the performance of the proposed method. We generated a real-time control code in MATLAB/Simulink to apply ControlDesk. The control algorithm was applied to the same simulink block used in the simulation. ControlDesk manages the overall experimental conditions, control parameters, and data acquisition. RapidPro was equipped with two "PS-HCHBD 2/2" power-stage modules. The maximum ratings of the power-stage modules were 30 V_{DC} and 19 A_{rms}. An incremental optical encoder (2500 lines/r) was used to measure the position. The control sampling rate was set to 20kHz. The powder brake generates a load torque against the velocity with a maximum value of 2N·m.

The experiments were conducted for the three conditions as follows:

- Condition 1: Without disturbances
- Condition 2: With the parameter uncertainties
- Condition 3: With parameter uncertainties and the load torque.

This article has been accepted for publication in a future issue of this journal, but has not been fully edited. Content may change prior to final publication. Citation information: DOI 10.1109/ACCESS.2021.3121127, IEEE Access

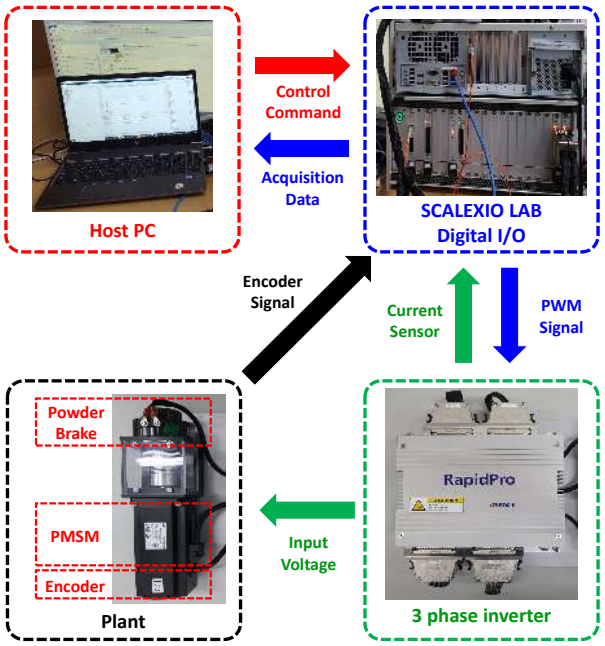

FIGURE 8: PMSM experimental setup

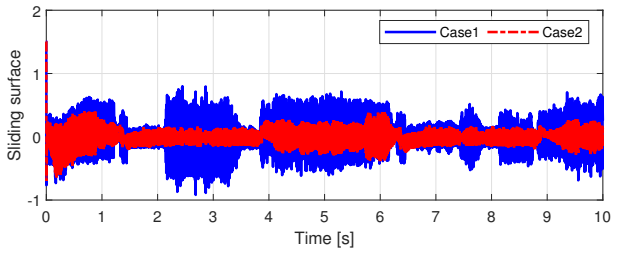

(a) Sliding surface s

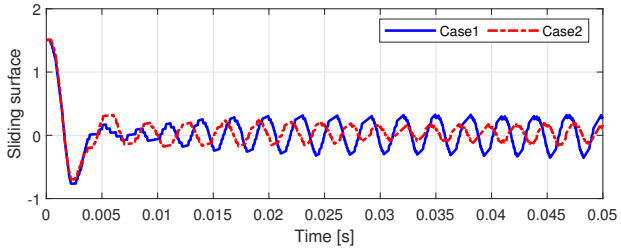

(b) Enlarged sliding surfaces

FIGURE 9: Sliding surfaces in Condition 1

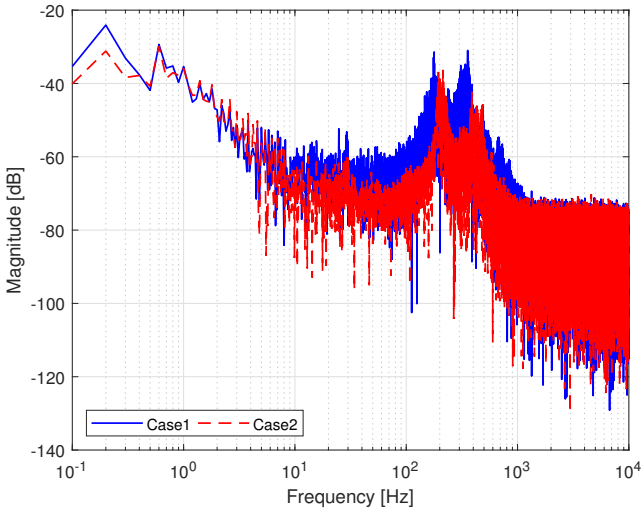

FIGURE 10: Frequency spectra of sliding surfaces in Condition 1

1) Condition 1: Without Disturbances

In these experiments, the nominal values listed in Table 1 were used for PMSMs. The sliding surfaces of Cases 1 and 2 are shown in Fig. 9. The chattering was more reduced by the STNGSMC in Case 2 than in Case 1. The frequency spectra of the sliding surfaces are presented in Fig. 10. We observe that near 200 Hz, the chattering of Case 2 was 3 dB smaller than that of Case 2. For the secondary harmonics frequency i.e., 460 Hz, the chattering was also reduced by 15 dB. The position tracking performances of Cases 1 and 2 are shown in Fig. 11. The ripple of the position in Case 2 was smaller than that in Case 1 because the chattering of the sliding surface in Case 2 was smaller than that in Case 1. The input currents are shown in Fig. 12. The input ripple in Case 2 is smaller than that in Case 1.

2) Condition 2: With the Parameter Uncertainties

To evaluate the robustness of the proposed method against parameter uncertainties, the experiments were tested with parameter uncertainties. The parameter uncertainties, which are a maximum of 20 % from the nominal value of Table 1, were applied, and the sliding surfaces are shown in Fig. 13. The chattering was more reduced by the STNGSMC in Case 2 than in Case 1. The frequency spectra of the sliding surfaces are shown in Fig. 14. We see that at 200 Hz, the chattering of Case 2 was 3 dB smaller than that of Case 2. For the secondary harmonics frequency, i.e., 460 Hz, the chattering was also reduced by 15 dB. The position tracking performances of Cases 1 and 2 are shown in Fig. 15. The ripple of the position in Case 2 was smaller than that in Case 1 because the chattering of the sliding surface in Case 2 was smaller than that in Case 1. The input currents are shown in Fig. 16. The input ripple in Case 2 is smaller than that in Case 1.

3) Condition 3: With parameter uncertainties and the load torque

To evaluate the robustness of the proposed method against parameter uncertainties and load torque, the experiments

This article has been accepted for publication in a future issue of this journal, but has not been fully edited. Content may change prior to final publication. Citation information: DOI 10.1109/ACCESS.2021.3121127, IEEE Access

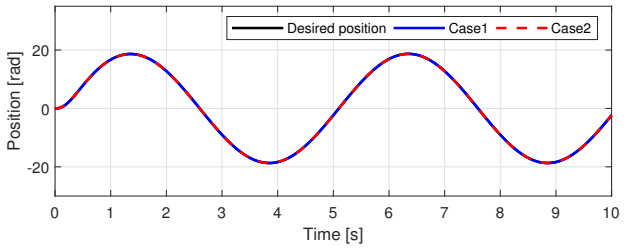

(a) Position tracking performances

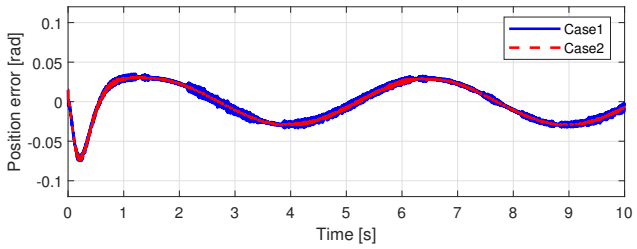

(b) Position tracking errors

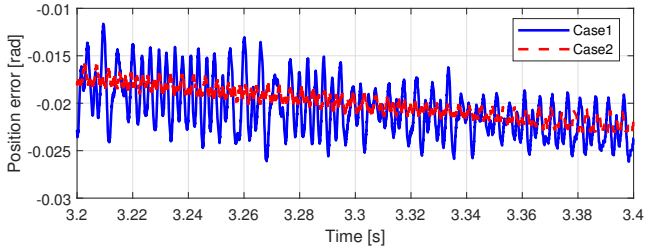

(c) Enlarged Position tracking errors

FIGURE 11: Position tracking performances in Condition 1

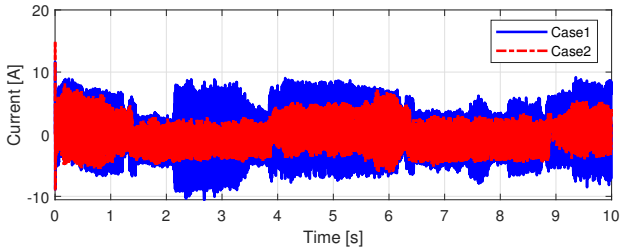

FIGURE 12: Current inputs in Condition 1

were tested with the parameter uncertainties and load torque. As shown in Fig. 17, a large load torque was applied. The sliding surfaces of Cases 1 and 2 are shown in Fig. 18. Owing to the large disturbance, including the parameter uncertainties and load torque, the chattering for Condition 3 increased more than that for Conditions 1 and 2. The chattering was more reduced by the STNGSMC in Case 2 than in Case 1. The frequency spectra of the sliding surfaces are presented in Fig. 14. We see that near 200 Hz, the chattering of Case 2 was 3 dB smaller than that of Case 2. The position tracking performances of Cases 1 and 2 are shown in Fig. 20. The ripple of the position in Case 2 was smaller than that in Case

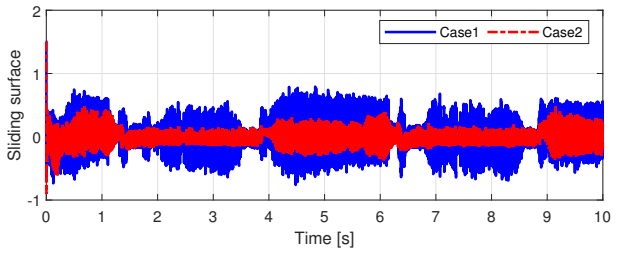

(a) Sliding surfaces s

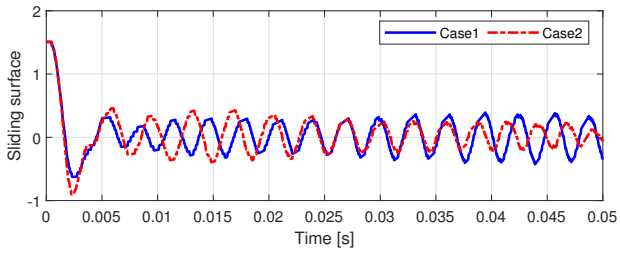

(b) Enlarged sliding surfaces

FIGURE 13: Sliding surfaces in Condition 2

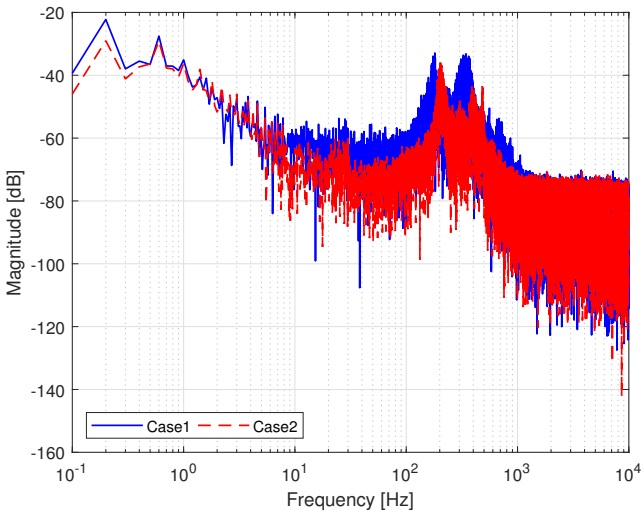

FIGURE 14: Frequency spectra of sliding surfaces in Condition 2

1 because the chattering of the sliding surface in Case 2 was smaller than that in Case 1. The input currents are shown in Fig. 21. The input oscillations are similar between Cases 1 and 2. However, the chattering and oscillation were reduced in Case 2.

V. CONCLUSION

In this paper, we proposed the STNGSMC to improve the position control performance of PMSMs, and the nonlinear gain was developed to improve the position tracking perfor-

This article has been accepted for publication in a future issue of this journal, but has not been fully edited. Content may change prior to final publication. Citation information: DOI 10.1109/ACCESS.2021.3121127, IEEE Access

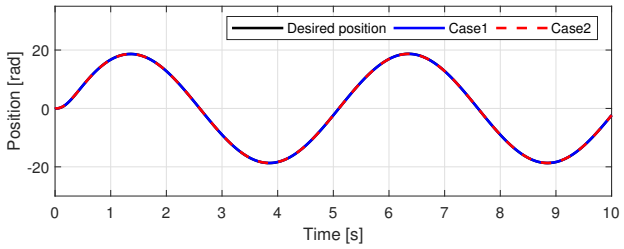

(a) Position tracking performances

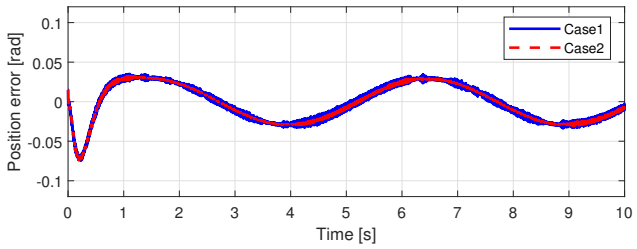

(b) Position tracking errors

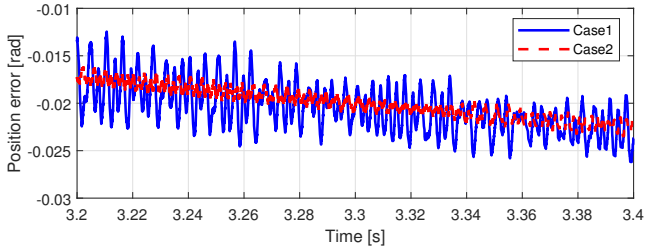

(c) Enlarged Position tracking errors

FIGURE 15: Position tracking performances in Condition 2

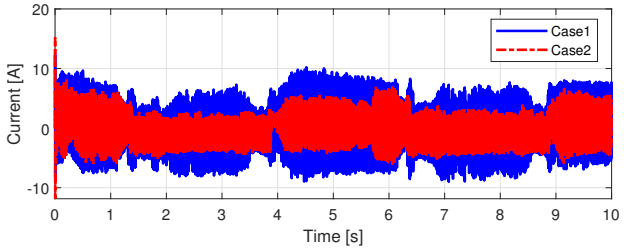

FIGURE 16: Current inputs in Condition 2

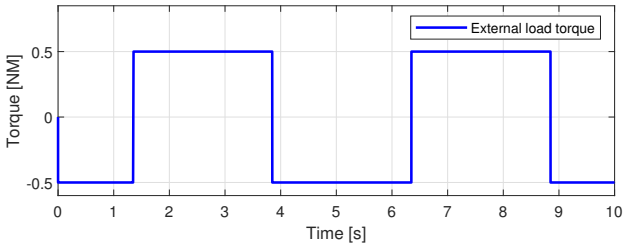

FIGURE 17: Injected load torque in Condition 3

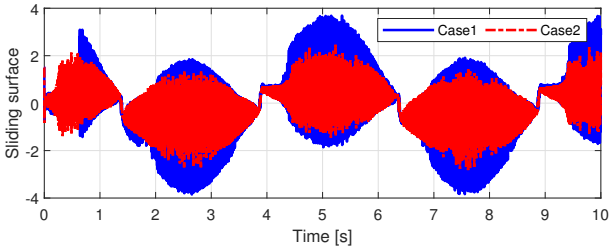

(a) Sliding surfaces s

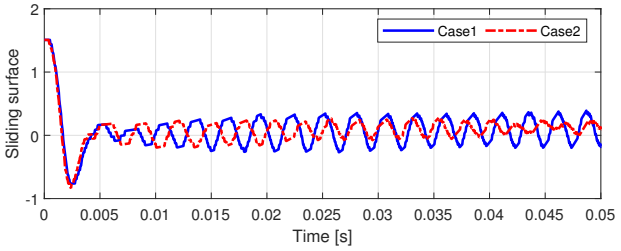

(b) Enlarged sliding surfaces

FIGURE 18: Sliding surfaces in Condition 3

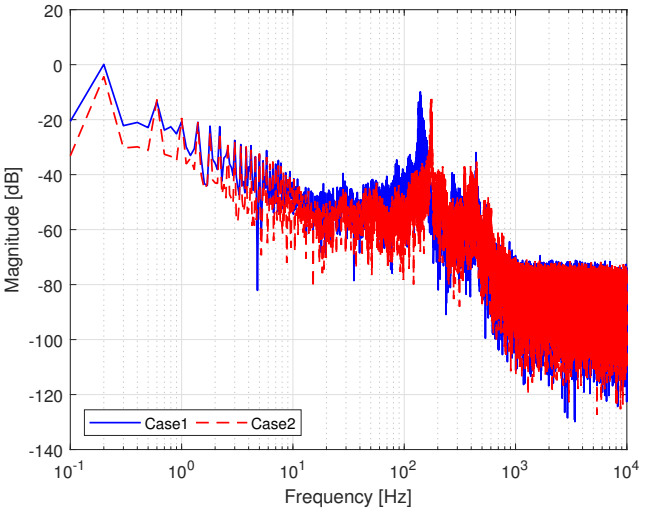

FIGURE 19: Frequency spectra of sliding surfaces in Condition 3

mance of the STSMC. The inclusion of nonlinear gain in the STSMC was demonstrated to reduce chattering. Based on the results obtained, we proved the stability of closed-loop systems using the Lyapunov theorem, and we experimentally verified the performance of the proposed method. The chattering phenomenon was calculated by describing function methods. The chattering was compared for conventional SMC, STSMC, and STNGSMC along with unmodeled dynamics, such as the PWM switching noise, sensor noise, and quantization effect. In the simulations and experiments, the STNGSMC reduced the chattering phenomenon in SMC. In Condition 1, the sine wave position reference was used without uncertainties. Furthermore, to evaluate the robustness of the proposed method, Condition 2 was conducted under parameter uncertainties, and in Condition 3, the load

This article has been accepted for publication in a future issue of this journal, but has not been fully edited. Content may change prior to final publication. Citation information: DOI 10.1109/ACCESS.2021.3121127, IEEE Access

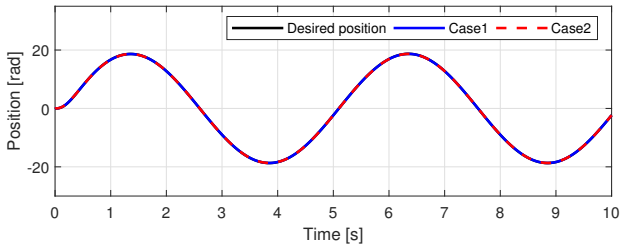

(a) Position tracking performances

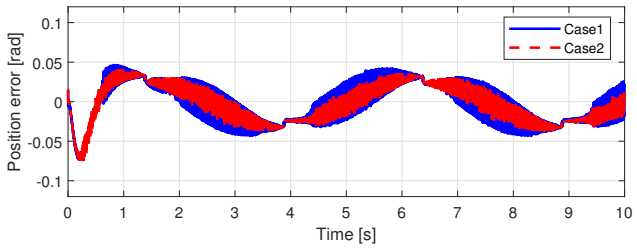

(b) Position tracking errors

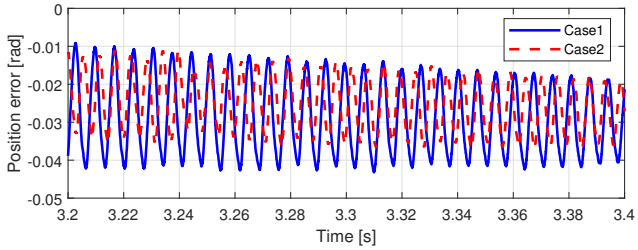

(c) Enlarged Position tracking errors

FIGURE 20: Position tracking performances in Condition 3

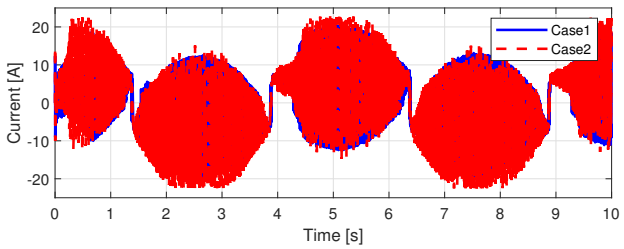

FIGURE 21: Current inputs in Condition 3

torque was applied. The robustness of the proposed method is mathematically proven in Section II. The chattering was reduced in the steady state because of nonlinear gain. Using the analysis of the frequency spectra, the chattering magnitude was reduced by 3 dB on average, which means that the chattering width of the proposed method was reduced by up to half that of STSMC. The simulation and experimental results demonstrated that the chattering width was observed in both the time domain and frequency spectra. The chattering affected the position tracking performance in transient and steady-state responses, and the simulation and experimental results demonstrate that position error ripples are reduced. A wide chattering width was observed in the experimental results owing to unmodeled dynamics. Therefore, a low oscillation was observed in the control input, which is the quadrature current.

REFERENCES

[1] J. Chiasson, *Modeling and High-performance Control of Electric Machnices*, 3rd ed. Willey &son Inc., 2005.

[2] R. Krishnan, *Electric Motor Drives: Modeling, Analysis, and Control*, Upper Saddle River, NJ, Unite States: Prentice-Hall, 2001.

[3] W. Kim, D. Shin and C. C. Chung "Microstepping with nonlinear torque modulation for permanent magnet stepper motors," *IEEE Trans. Contr. Syst. Technol.*, Vol. 21 , No. 5, pp. 1971-1979, Sep., 2013.

[4] V. Petrovic, R. Ortega, A. M. Stankovic and G. Tadmor, "Design and implementation of an adaptive controller for torque ripple minimization in PM synchronous motors," *IEEE Trans. Power Electron.,* vol. 15, no. 5, pp. 871-880, Sep., 2000.

[5] Y. Lee, J. Gil and W. Kim "Velocity control for sideband harmonics compensation in permanent magnet synchronous motors with low switching frequency inverter," *IEEE Trans. Ind. Electron.,* vol. 68, no. 4, pp. 3434-3444, Apr. 2021.

[6] S. Barkat, A. Tlemcani and H. Nouri, "Noninteracting adaptive control of pmsm using interval type-2 fuzzy logic systems," *IEEE Trans. on Fuzzy Systems,* vol. 19, no. 5, pp. 925-936, Oct., 2011.

[7] Y. Kung and M. Tsai, "FPGA-based speed control ic for pmsm drive with adaptive fuzzy control," *IEEE Trans. Power Electron.,* vol. 22, no. 6, pp. 2476-2486, Nov., 2007.

[8] J. Linares-Flores, C. Garcia-Rodriguez, H. Sira-Ramirez and O. D. Ramirez-Cardenas, "Robust backstepping tracking controller for low-speed PMSM positioning system: design, analysis, and implementation," *IEEE Trans. Ind. Inform.,* vol. 11, no. 5, pp. 1130-1141, Oct., 2015.

[9] L. Li, J. Xiao, Y. Zhao, K. Liu, X. Peng, H. Luan, and K. Li, "Robust position anti-interference control for PMSM servo system with uncertain disturbance," *CES Trans. Elect. Mach. and Syst.,* vol. 4, no. 2, pp. 151-160, Jun., 2020.

[10] K. Belda and D. Vosmik, "Explicit generalized predictive control of speed and position of PMSM drives," *IEEE Trans. Ind. Electron.,* vol. 63, no. 6, pp. 3889-3896, Jun., 2016.

[11] M. Preindl and S. Bolognani, "Model predictive direct speed control with finite control set of PMSM-VSI drive systems," *2011 Workshop on Predictive Control of Elect. Drives Power Electron.,* Munich, Germany, 2011, pp. 17-23.

[12] F. F. M. El-Sousy, "Intelligent optimal recurrent wavelet elman neural network control system for permanent-magnet synchronous motor servo drive," *IEEE Trans. Ind. Inform.,* vol. 9, no. 4, pp. 1986-2003, Nov., 2013.

[13] K. Shyu, C. Lai, Y. Tsai and D.-I. Yang, "A newly robust controller design for the position control of permanent-magnet synchronous motor," *IEEE Trans. Ind. Electron.,* vol. 49, no. 3, pp. 558-565, Jun., 2002.

[14] S. Li, M. Zhou and X. Yu, "Design and implementation of terminal sliding mode control method for PMSM speed regulation system," *IEEE Trans. Ind. Inform.,* vol. 9, no. 4, pp. 1879-1891, Nov., 2013.

[15] K. Zhao, T. Yin, C. Zhang, J. He, X. Li, Y. Chen, R. Zhou, and A. Leng, "Robust model-free nonsingular terminal sliding mode control for pmsm demagnetization fault," *IEEE Access,* vol. 7, pp. 15737-15748, Jan., 2019.

[16] Z. Yin, L. Gong, C. Du, J. Liu and Y. Zhong, "Integrated position and speed loops under sliding mode control optimized by differential evolution algorithm for PMSM drives," *IEEE Trans. Power Electron.,* vol. 34, no. 9, pp. 8994-9005, Sep., 2019.

[17] X. G. Zhang, L. Z. Sun, K. Zhao, and L. Sun, " Nonlinear speed control for PMSM system using sliding-mode control and disturbance compensation techniques,"*IEEE Trans. Power Electron.*, vol. 28, pp.1358-1365, Mar., 2013.

[18] S. Shin, D. Shin, Y. Lee, and C. C. Chung, "Sliding mode control based on singular perturbation theory for position tracking of permanent magnet stepper motors,"*in Proc. Int. Conf. Control Automat. Syst.*, 2013, pp. 767-770.

[19] I. C. Baik, K. H. Kim, and M. J. Youn, "Robust nonlinear speed control of PM synchronous motor using boundary layer integral sliding mode control technique," *IEEE Trans. Control Syst. Technol.,* vol. 8, pp. 47-54, Jan., 2000.

[20] J. Liu, H. Li and Y. Deng, "Torque ripple minimization of PMSM nased on robust ILC via adaptive sliding mode control," *IEEE Trans. Power Electron.,* vol. 33, no. 4, pp. 3655-3671, Apr., 2018.
[21] D. Liang, J. Li, R. Qu, and W. Kong, "Adaptive second-order sliding-mode observer for PMSM sensorless control considering VSI nonlinearity," *IEEE Trans. Power Electron.,* vol. 33, no. 10, pp. 8994-9004, Oct. 2018.
[22] Y. Shtessel, C. Edwards, L. Fridman and A. Levant, *Sliding Mode Control and Observation*, Birkhauser, New York, 2014.
[23] A. Levant, "Sliding order and sliding accuracy in sliding mode control," *Int. J. Control,* vol. 58, no. 6, pp. 1247-1263, Aug., 1993.
[24] Z. Li, S. Zhou, Y. Xiao, and L. Wang, "Sensorless vector control of permanent magnet synchronous linear motor based on self-adaptive super-twisting sliding mode controller," *IEEE Access,* vol. 7, pp. 44998-45011, Apr., 2019.
[25] Q. Hou and S. Ding, "GPIO based super-twisting sliding mode control for PMSM," *IEEE Trans. Circuits Syst. II: Express Briefs,* [Online:] 10.1109/TCSII.2020.3008188.
[26] Q. Hou, S. Ding and X. Yu, "Composite super-twisting sliding mode control design for PMSM speed regulation problem based on a novel disturbance observer," *IEEE Trans. Energy Conversion*, [Online:] DOI: 10.1109/TEC.2020.2985054.
[27] Y. B. Shtessel, J. A. Moreno, F. Plestan, L. M. Fridman, and, A. S. Poznyak, "Super-twisting adaptive sliding mode control: A Lyapunov design," In Proc. IEEE Conf. Dec. Control, 2010, 5109-5113.
[28] T. Gonzalez, J. A. Moreno, and L. Fridman. "Variable gain super-twisting sliding mode control," *IEEE Trans. Autom. Control,* vol. 57, no. 8, pp. 2100-2105, 2011.
[29] A. Swikir and V. Utkin, "Chattering analysis of conventional and super twisting sliding mode control algorithm," *2016 14th Int. Workshop on Variable Structure Syst. (VSS),* Nanjing, China, 2016, pp. 98-102.
[30] V. Utkin, "On convergence time and disturbance rejection of super-twisting control," *IEEE Trans. Autom. Control,* vol. 58, no. 8, pp. 2013-2017, Aug. 2013.
[31] H. Khalil, *Nonlinear Systems*, 3rd ed. Upper Saddle River, NJ: Prentice-Hall, 2002.
[32] J. A. Moreno and M. Osorio, "Strict lyapunov functions for the super-twisting algorithm," *IEEE Trans. Automat. Control*, vol. 57, no. 4, pp. 1035-1040, Apr. 2012.
[33] A. Levent, "Robust exact differentiation via sliding mode technique," *Automatica*, vol. 34, pp. 379-384, 1998.

JEONGHWAN GIL was born in Ulsan, Korea. He received the B.S. degree in electronic engineering in Gachon Univ. and the M.S. degree in electrical engineering from Hanyang University, Seoul, South Korea, in 2014 and 2017, respectively. He was studying in department of energy system engineering in Chung-Ang University, Seoul, South Korea, from 2018.His research interests include nonlinear control and observer, sliding mode control, as well as their industrial applications.

SESUN YOU received the B.S. degree from the School of Energy Systems Engineering, Chung-Ang University, Seoul, South Korea, in 2020. He is currently pursuing the Ph.D. degree with the Department of Energy Systems Engineering, Chung-Ang University, Seoul. His research interests include nonlinear control, adaptive control, neural network based control, intelligent control for nonlinear systems, and their industrial applications.

YOUNGWOO LEE received the B.S. degree from Chungbuk National University, Cheongju, Korea, in 2010, and the Ph.D. degree from Hanyang University, Seoul, Korea, in 2017, both in electrical engineering. From 2017 to 2018, he was a Research Scientist with the Ulsan National Institute of Science Technology, and a Postdoctoral Researcher with the Department of Mechanical Engineering, University of California, Berkeley, CA, USA. From 2018 to 2019, he was with the Memory Division, Samsung Electronics Ltd., Korea. From 2019 to 2020, he was an Assistant Professor with the Department of Electronics Engineering, Pai Chai University, Daejeon, Korea. In 2020, he joined the Faculty of Chonnam National University, Gwangju, Korea. His main research interests include power system optimization, electric machine control, nonlinear and optimal controller design.

WONHEE KIM received the B.S. and M.S. degrees in electrical and computer engineering and the Ph.D. degree in electrical engineering from Hanyang University, Seoul, South Korea, in 2003, 2005, and 2012, respectively. From 2005 to 2007, he was with Samsung Electronics Company, Suwon, South Korea. In 2012, he was with the Power and Industrial Systems Research and Development Center, Hyosung Corporation, Seoul, South Korea. In 2013, he was a Post-Doctoral Researcher with the Institute of Nano Science and Technology, Hanyang University, Seoul, South Korea, and a Visiting Scholar with the Department of Mechanical Engineering, University of California, Berkeley, CA, USA. From 2014 to 2016, he was with the Department of Electrical Engineering, Dong-A University, Busan, South Korea. He is currently an Associate Professor with the School of Energy Systems Engineering, Chung-Ang University, Seoul, South Korea. His current research interests include nonlinear control and nonlinear observers, as well as their industrial applications.